Acta Crystallographica Section B
Structural Science
ISSN 0108-7681

Isosymmetrical phase transition in α-YbV_4O_8

Karen Friese,[a]* Yasushi Kanke,[b] Andy N. Fitch,[c] Wolfgang Morgenroth[d] and Andrzej Grzechnik[a]

[a]Departamento Física Materia Condensada, Facultad de Ciencia y Tecnología, Universidad del País Vasco, Apdo. 644, 48080 Bilbao, Spain, [b]Advanced Nano Materials Laboratory, National Institute for Materials Science, 1-1 Namiki, Tsukuba, Ibaraki 305-0044, Japan, [c]Materials Science Group, European Synchrotron Radiation Facility, BP220, F-38043 Grenoble CEDEX, France, and [d]Department of Chemistry, Aarhus University, Denmark

Correspondence e-mail: karen.friese@ehu.es

Received 11 June 2008
Accepted 13 August 2008

The structure of YbV_4O_8 is related to the $CaFe_2O_4$ structure type. VO_6 octahedra form a three-dimensional framework with tunnels in which the Yb^{3+} ions are incorporated. Two different polymorphs α and β are known and differ mainly in the arrangement of the Yb ions within the framework. We studied the structure and magnetic properties of α-YbV_4O_8 as a function of temperature. At approximately 70 K α-YbV_4O_8 undergoes a first-order isosymmetrical phase transition ($P2_1/n \rightarrow P2_1/n$). While in the high-temperature α phase the three V^{3+} and one V^{4+} are disordered over the four symmetrically independent octahedral sites, in the low-temperature α' phase complete charge ordering is observed. The transition is accompanied by a paramagnetic–paramagnetic anomaly in the magnetic susceptibility data which can be interpreted on the basis of spin-gap formation. The transition mechanism in the α polymorph is very similar to that observed earlier in the β polymorph at 185 K.

1. Introduction

The interplays of charge, magnetic and structural order–disorder are of keen interest. Mixed-valence vanadates of the composition LnV_4O_8 are ideal systems in this respect, as complex phenomena such as (iso)structural phase transitions, charge ordering or polytypism are observed.

LnV_4O_8 compounds (Ln = Y, Yb) can be described as superlattice structures of well known orthorhombic $CaFe_2O_4$. VO_6 octahedra share common edges and form a three-dimensional framework with tunnels along the [001] direction. The V_4O_8 framework is essentially identical with the corresponding Fe_2O_4 framework in $CaFe_2O_4$. However, the Ln^{3+} cations, which occupy half of the Ca^{2+} sites, are incorporated in two different types of ordering schemes, resulting in two polymorphs, denoted α and β (Kanke & Kato, 1997). The *c*-lattice parameters of both polymorphs are doubled when compared with the corresponding parameter of $CaFe_2O_4$.

In both the α and β phases, the Ln^{3+} cations form pseudocentered nets parallel to (010) (Fig. 1). In the β phases these nets are stacked with a stacking vector of $(b + c)/4$ or $(b - c)/4$, while in the α phases the stacking vectors alternate in a zigzag sequence (Figs. 1 and 2). This difference in stacking sequence leads to different monoclinic distortions, with the angle $\beta \neq 90^\circ$ in the α phase (space group $P12_1/n1$) and the angle $\alpha \neq 90^\circ$ in the β phase (space group $P2_1/n11$). To directly compare the two polymorphs, the *b*-lattice parameter of the β phase has to be doubled with respect to the α phase, resulting in a description of the structure in the non-standard setting $A2_1/d11$.

The similarity of the framework favors the occurrence of intergrowths of both phases within one crystal (Fig. 2; Friese *et*

al., 1997; Onoda *et al.*, 2003), making these compounds typical representatives of polytypic compounds.

In general, polytypism and stacking disorder are phenomena frequently observed in layered magnetic materials. Usually little is known about the underlying domain structures, yet the characteristic features related to the one-dimensional disorder in YbV_4O_8 (Kato *et al.*, 1997; Friese *et al.*, 1997; Onoda *et al.*, 2003) and YV_4O_8 (Onoda *et al.*, 2003) are very well studied.

The two polymorphs of YbV_4O_8 and YV_4O_8 co-exist over a wide temperature range and it has been shown that this fact can be interpreted on the basis of polytypic one-dimensional disorder: the β-phase polymorph is always twinned and the structure of the intermediate region from one twin domain to the next one is achieved by intergrown regions which possess the structure of the α-phase polymorph (Fig. 2).

All the accumulated knowledge about LnV_4O_8 compounds provides the ideal basis to study the interplay of magnetic anomalies, structural distortions and underlying domain structures as a function of temperature. These studies are further warranted by the fact that specific heat and magnetic susceptibility measurements indicate structural and magnetic transitions both for the α and the β polymorph, albeit at considerably different temperatures.

Recently, our results on β-YbV_4O_8 [lattice parameters at 290 K: a = 9.030 (5), b = 21.44 (3), c = 5.752 (2) Å, α = 89.911 (3)°, space group $A2_1/d11$; Kanke & Kato, 1997] demonstrated the existence of an isosymmetrical, first-order phase transition with discontinuous changes in the lattice parameters and large shifts of the atoms at 185 K (Friese *et al.*, 2007). In general, temperature-induced isosymmetrical phase transitions are rare, although recently comparable transitions were reported for multiferroic hexagonal manganites $RMnO_3$, where R = Y, Lu (Lee *et al.*, 2008). In β-YbV_4O_8 the transition is accompanied by a paramagnetic–paramagnetic anomaly which seems to involve spin-singlet formation (Friese *et al.*, 2007). Furthermore, we could show that the isosymmetrical transition in β-YbV_4O_8 is related to a complete charge ordering of the three V^{3+} and one V^{4+}: above the transition temperature (185 K) the trivalent and tetravalent V are disordered over the four symmetrically independent octahedral sites, below the phase transition the bond-valence sums indicate that they are completely ordered. While examples of partially ordered systems are frequent and involve important representatives like *e.g.* $Ln_{1-x}A_xMnO_3$ [Ln = rare earth, A = alkaline earth (Rao *et al.*, 1998; Radaelli *et al.*, 1997; Daoud-Aladine *et al.*, 2002; Goff & Attfield, 2004; Nagaev, 2002)], $CaFeO_3$ (Woodward *et al.*, 2000), $YBaCo_2O_5$ (Vogt *et al.*, 2000), $YNiO_3$ (Alonso *et al.*, 1999) or Fe_3O_4 (Berry *et al.*, 1998; Samiullah, 1995), the complete charge ordering observed in β-YbV_4O_8 seems to be rather unique.

Given the unusual phenomena observed in β-YbV_4O_8, we then studied the temperature dependence of the structure and magnetic properties of the α-phase polymorph (space group $P12_1/n1$; lattice parameters at 290 K: a = 9.0648 (3), b = 10.6215 (4), c = 5.7607 (1) Å, β = 90.184 (3)°; Kanke & Kato, 1997).

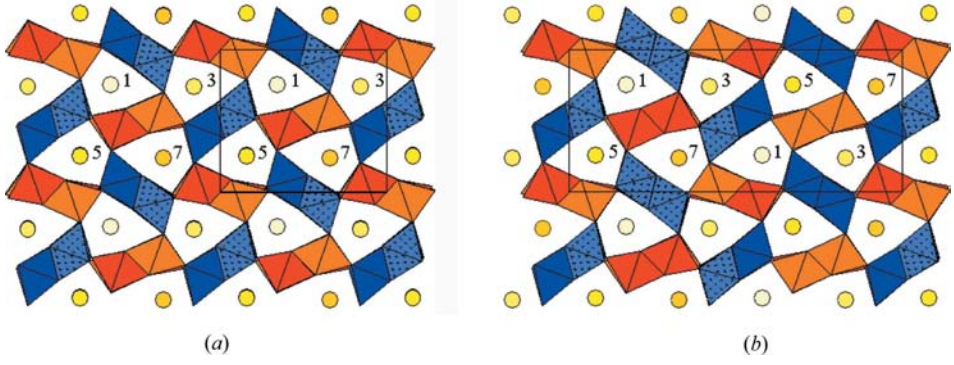

Figure 1
Structure of the (*a*) α and (*b*) β polymorph of YbV_4O_8. Octahedra around V are indicated. Octahedra which incorporate V^{4+} in the low-temperature phases are shown as dotted regions. Heights of Yb^{3+} ions are given in $x/8$.

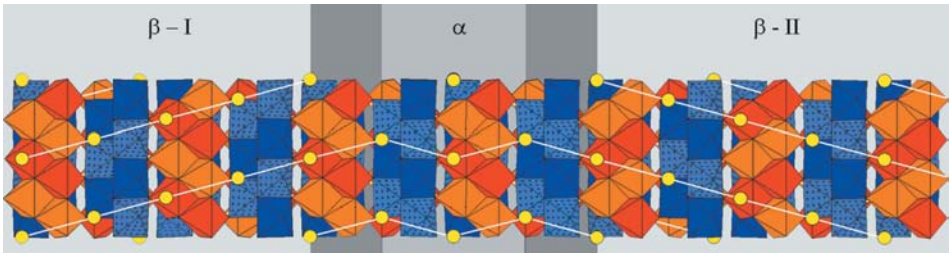

Figure 2
Polytypism in YbV_4O_8. Two β-phase domains in the twin relationship are shown. The structure of the intermediate region corresponds to the structure of α-YbV_4O_8.

2. Experimental

The single crystal of α-YbV_4O_8 is the same as that used for the earlier structure determination at ambient conditions (Kanke & Kato, 1997). The powder sample has been newly synthesized at a temperature of 1623 K according to the description given in Kanke & Kato (1997) using $YbVO_3$, $YbVO_4$ and V_2O_3 as starting materials. Magnetic susceptibility data were obtained with a magnetic property measurement system (MPMS) from Quantum Design in the temperature range 2–300 K (Fig. 3). The data were obtained with external fields of 0.1 and 5.0 T (both zero-field-cooled and field-cooled).

High-resolution X-ray powder diffraction experiments were carried out at the beamline ID31 of the European Synchrotron

Table 1
Crystal data and experimental details for α and α'-YbV_4O_8.

Crystal data	
Chemical formula	YbV_4O_8
μ_r	504.8
Cell setting, space group	Monoclinic, $P12_1/n1$
Z	4
Radiation type	Synchrotron
Wavelength (Å)	0.47686
Crystal form, colour	Irregular, black
Crystal size (mm^3)	0.004189
Data collection	
Diffractometer	Huber 4-Circle, Beamline D3, HASYLAB
Data collection method	φ scans
Absorption correction	Numerical
Criterion for observed reflections	$I>3\sigma(I)$
Refinement	
Refinement on	F
Weighting scheme	Based on measured s.u.s, $w = 1/[\sigma^2(F) + 0.0001(F^2)]$
Extinction method	B–C type 1 Gaussian isotropic (Becker & Coppens, 1974)
No. of parameters	119

Temperature (K)	250	200	150	100	65	50	8
a (Å)	9.0677 (3)	9.0651 (3)	9.0641 (3)	9.0675 (3)	9.0616 (5)	9.0469 (4)	9.0461 (3)
b (Å)	10.6261 (4)	10.6239 (4)	10.6229 (4)	10.6264 (4)	10.6244 (8)	10.6159 (4)	10.6156 (4)
c (Å)	5.7599 (2)	5.7539 (3)	5.7487 (3)	5.7473 (3)	5.7497 (4)	5.7814 (3)	5.7812 (3)
β (°)	90.185 (2)	90.182 (3)	90.182 (3)	90.190 (2)	90.292 (5)	90.065 (4)	90.068 (3)
V (Å^3)	554.99 (3)	554.14 (4)	553.52 (4)	553.78 (4)	553.54 (6)	555.25 (4)	555.17 (4)
θ_{max} (°)	32.62	32.60	32.60	32.59	31.79	31.82	31.83
No. of unique reflections	6594	6568	6572	6567	5954	5965	5970
D_x (g cm^{-3})	6.040	6.0498	6.056	6.053	6.055	6.037	6.038
μ (mm^{-1})	7.886	7.898	7.906	7.903	7.906	7.882	7.883
T_{min}	0.6585	0.6583	0.6690	0.7072	0.7083	0.7082	0.7083
T_{max}	0.7792	0.7793	0.8216	0.7851	0.7849	0.7856	0.7863
No. of measured reflections	51 399	68 351	62 291	54 937	53 984	60 438	54 380
No. of independent reflections	6594	6568	6572	6567	5954	5965	5970
No. of observed reflections	5676	5851	5643	5646	5290	4931	5254
R_{int}	0.056	0.053	0.056	0.050	0.042	0.052	0.049
$R[F > 3\sigma(F)]$	0.032	0.033	0.033	0.033	0.033	0.031	0.030
$wR(F)$	0.034	0.039	0.038	0.036	0.044	0.037	0.037
S	1.87	2.11	1.74	1.92	1.54	1.52	1.47
$(\Delta/\sigma)_{max}$	0.074	0.058	0.032	0.031	−0.039	0.016	−0.041
$\Delta\rho_{max}$	3.53	3.99	5.00	5.55	4.52	3.91	3.83
$\Delta\rho_{min}$	−8.52	−8.96	−7.65	−8.82	−6.15	−5.71	−5.91
Extinction coefficent	0.34 (2)	0.31 (3)	0.33 (3)	0.26 (3)	0.28 (5)	0.30 (3)	0.32 (3)

Computer programs used: *JANA*2006 (Petříček *et al.*, 2006).

Radiation Facility, Grenoble, France, using a wavelength of 0.3995 Å. A continuous scan with a speed of 2.5° min^{-1} was used; scan limits in 2θ were $-5 \leq 2\theta \leq 20°$. The beamline is equipped with nine detectors, which have an offset of 2° in 2θ with respect to each other. The limits given refer to the central detector. Diagrams were measured in 10 K steps between 290 and 100 K and in 5 K steps between 100 and 10 K. For cooling a He-flow cryostat from Janis Inc., USA, was used. Lattice parameters were extracted using the LeBail method (LeBail *et al.*, 1988) with the program *JANA*2006 (Petříček *et al.*, 2006).

Single-crystal diffraction data were measured at a wavelength of 0.47686 Å at the beamline D3 of the HASYLAB on a Huber four-circle diffractometer in combination with a MARCCD 165 detector. Temperatures for the measurements were 250, 200, 150, 100, 65, 50 and 8 K. For cooling N_2 and He cryostats were employed (Cryojet and Helijet from Oxford Diffraction). Single-crystal structure refinements were carried out with the program *JANA*2006 (Petříček *et al.*, 2006). Further details of the data collection and refinement are summarized in Table 1.[1]

3. Results

3.1. Magnetic susceptibility

The magnetic susceptibility data of α-YbV_4O_8 show a pronounced anomaly around 70 K and a further smaller anomaly at approximately 7 K (Fig. 3), both of which have to be attributed exclusively to α-YbV_4O_8 as powder diffraction experiments show the sample to be free from impurities. Indeed, the fact that the magnetic susceptibility decreases abruptly below approximately 70 K confirms that the specimen is free from ferromagnetic impurities such as $Yb_2V_2O_7$ pyrochlore. The pair of 0.1 T data, zero-field-cooled and field-cooled, does not show any significant difference, indicating that the compound is free from ferromagnetic order in the measured temperature range.

The magnetic susceptibility virtually obeys Curie–Weiss paramagnetism in the two temperature regions above and below the anomaly at 70 K, which is obvious from the nearly linear relationship between the inverse magnetic susceptibility and the temperature (Fig. 3). Both regions show a positive $1/\chi$ intercept reflecting negative Weiss temperatures and antiferromagnetic interactions. The slope is larger for the low-temperature region than for the high-temperature one, which indicates that the Curie–Weiss moment decreases below the anomaly at 70 K. The results of the analysis of the magnetic data are summarized in Table 2.

[1] Supplementary data for this paper are available from the IUCr electronic archives (Reference: SN5072). Services for accessing these data are described at the back of the journal.

The Curie constant of 4.43 (4) emu K^{-1} mol^{-1} for the high-temperature region corresponds to an intermediate value for one cation with $^2F_{7/2}$ (p_{eff} = 4.54, C = 2.57 emu K^{-1} mol^{-1}), one cation with S = 1 (p_{eff} = 2.83, C = 1.00 emu K^{-1} mol^{-1}) and three cations with S = 1/2 (p_{eff} = 1.73, C = 0.375 emu K^{-1} mol^{-1}) per unit formula, on the one hand (4.70 emu K^{-1} mol^{-1}), and one cation with $^2F_{7/2}$ and four cations with S = 1/2 per unit formula on the other hand (4.07 emu K^{-1} mol^{-1}). As will be explained later, the bond-valence sums and Madelung energy calculations indicate that the four V sites show an essentially uniform charge distribution above 70 K. One possible explanation for the spin state above 70 K is as follows. Yb^{3+} exhibits the $^2F_{7/2}$ state. At least three of the four V sites show a local moment of S = 1/2. The remaining V site exhibits either a local moment of S = 1/2 or S = 1. The S = 1 moment, if any, is randomly distributed among the four V sites. The remaining three (or two) 3*d* electrons per unit formula are delocalized over the four V sites. The magnetic characters in α-YbV_4O_8 are thus essentially the same as those of β-YbV_4O_8 above 185 K.

The Curie constant of 2.90 (12) emu K^{-1} mol^{-1} obtained from the low-temperature region is larger than the theoretical value for Yb^{3+} (2.57 emu K^{-1} mol^{-1}). However, the difference Curie constant, 2.90–2.57 = 0.33 emu K^{-1} mol^{-1}, is too small to be attributed to the three V^{3+} and one V^{4+} per unit formula. This suggests possible spin-singlet formation in the low-temperature phase of the α' polymorph.

3.2. Diffraction experiments

Fig. 4 shows an excerpt of a Guinier representation based on 38 temperature-dependent powder diffraction diagrams of α-YbV_4O_8. At approximately 70 K a first-order phase transition is clearly visible. No additional reflections appear below the phase transition temperature, yet the position of the diffraction peaks are significantly shifted in the low-temperature phase. High- and low-temperature phases coexist in the temperature range between approximately 65 and 75 K. The diffraction diagrams can be indexed assuming the monoclinic space group $P2_1/n$ both for the high-temperature α and the low-temperature α' phase, indicating the isosymmetrical character of the transition.

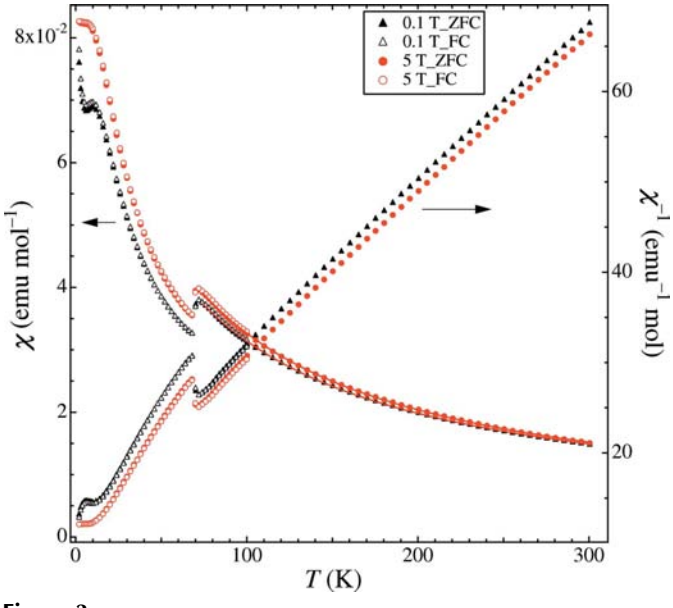

Figure 3
Magnetic susceptibility and inverse magnetic susceptibility of α-YbV_4O_8 obtained with external fields of 0.1 and 5.0 T (both zero-field-cooled and field-cooled).

Table 2
Curie constant C, Weiss temperature θ, and temperature-independent susceptibility χ_0 of α-YbV_4O_8 obtained from the zero-field-cooled 5 T data.

C (emu K mol^{-1})	θ (K)	χ_0 (emu mol^{-1})	Temperature range analyzed (K)
4.43 (4)	−46.2 (9)	0.00239 (11)	$74 \le T \le 300$
2.90 (12)	−23.6 (12)	0.0032 (10)	$18 \le T \le 64$

Fig. 5 shows the corresponding lattice parameter as a function of temperature extracted *via* the LeBail method (LeBail *et al.*, 1988) with the program *JANA*2006 (Petříček *et al.*, 2006). At the transition from the α to the α' phase the unit-cell volume is increased by approximately 0.25%. This effect can be mainly attributed to a large increase of the *c* lattice parameters (>0.5%). On the other hand, both the *a* and *b* lattice parameters, as well as the monoclinic angle decrease slightly at the transition.

As can be seen in Fig. 5 the lattice parameters of the high-temperature α phase do not behave smoothly as a function of temperature and even show a small additional anomaly at approximately 150 K, which is not reflected in the single-crystal nor in the magnetic data. We have as yet no explanation for this fairly strange behavior of the lattice parameters. Refinements of the lattice parameters using peak positions

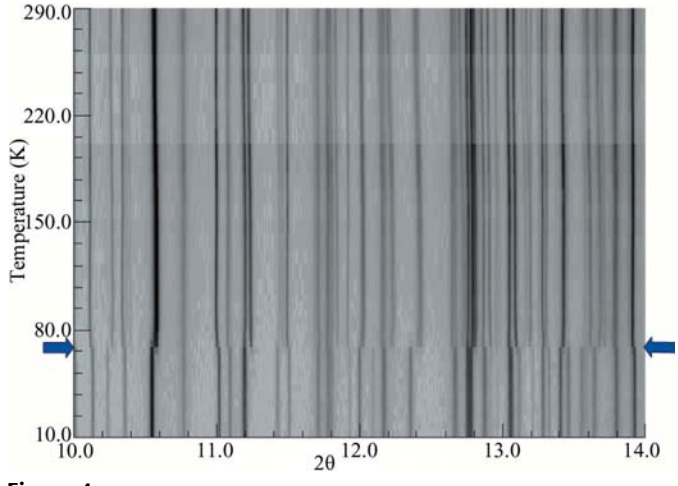

Figure 4
Excerpt of a Guinier representation of the powder diffraction diagram of α-YbV_4O_8 as a function of temperature; the simulation is based on 38 individual powder diffraction scans. Only the range $10 < 2\theta < 14°$ is shown for reasons of clarity. Simulation made with the program *Powder3D* (Hinrichsen *et al.*, 2006).

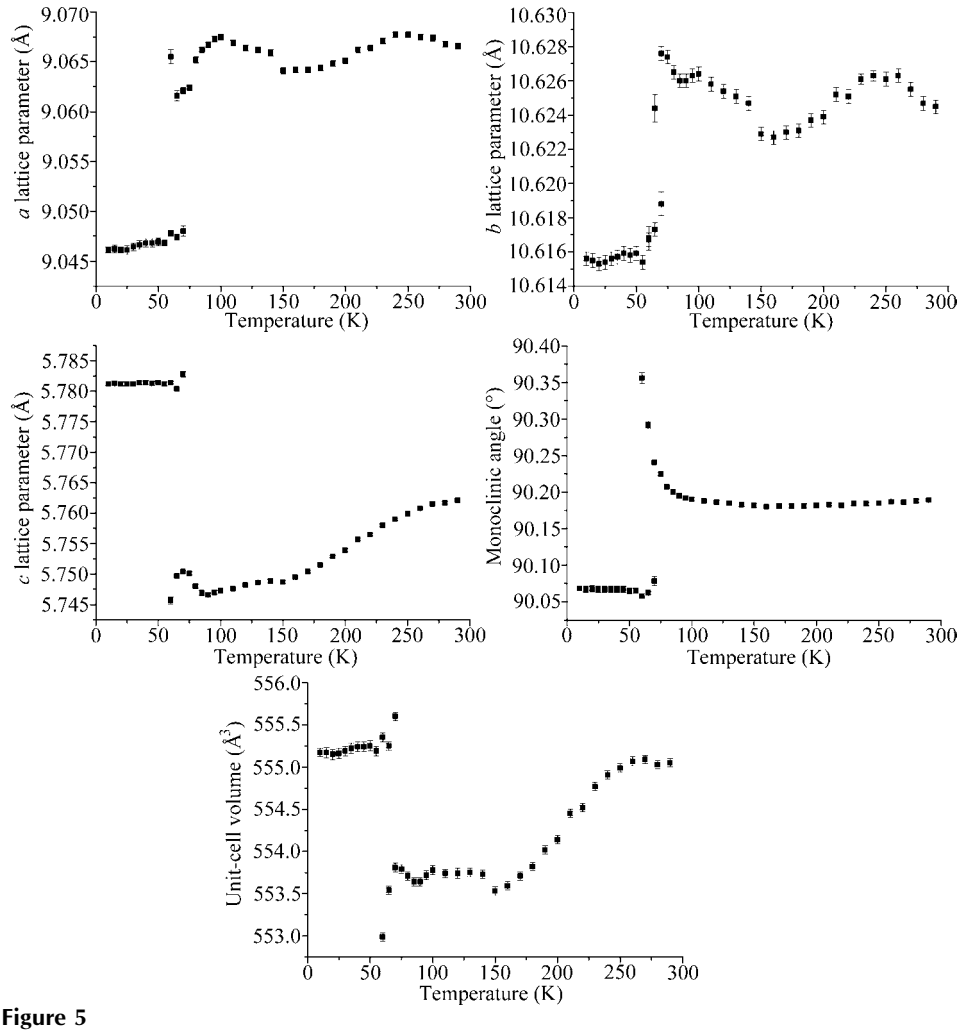

Figure 5
Lattice parameters and unit-cell volume of α-YbV_4O_8 from synchrotron powder diffraction data as a function of temperature. Standard deviations are indicated by error bars.

extracted through individual peak fitting confirm the values obtained from the LeBail refinement. This might be an indication that the observed variations are rather intrinsic to the sample than attributable to an unidentified systematic error.

To characterize the structural changes at the $\alpha \rightarrow \alpha'$ transition in more detail we measured single-crystal diffraction data as a function of temperature. The refinements carried out with the program *JANA*2006 (Petříček *et al.*, 2006) confirm the space group $P2_1/n$ for both the α and α' phase.

Although most of the atoms are affected by the transition and nearly all geometrical parameters such as bond distances and angles change discontinuously at the transition, the effect on the $V4O_6$ octahedron is especially striking. This octahedron shrinks considerably in volume at the transition to the low-temperature phase, a fact that is reflected in the strong decrease of the average V—O distance in this octahedron (Fig. 6). At the same time, the average distances for the other three VO_6 octahedra increase slightly. Examination of the corresponding bond-valence sums calculated according to Brese & O'Keeffe (1991) and using the empirical parameters for V^{3+} and V^{4+}, respectively, clearly demonstrates that the mechanism of the phase transition in the α compound is equivalent to the mechanism in the corresponding β phase: above the phase transition temperature the three V^{3+} and one V^{4+} are disordered over the four symmetry-independent sites, although there is a slightly more elevated charge on the V4 site than on the remaining three sites.[2] After the phase transition V^{4+} is fully concentrated on the V4 site, while the three V^{3+} ions are incorporated into the remaining three octahedra (Fig. 6).

Fig. 7(*a*) shows the shifts of the V4 and O5 atoms as a function of temperature. As can be seen, the displacement is extremely large for the O5 atom (>0.1 Å; Fig. 7). In the bottom part of the figure the individual V4—O distances, normalized with the average distances at the corresponding temperature, are portrayed. One can clearly see the strong shortening of V4—O5, which leads to the formation of a vanadyl group characteristic for V^{4+}. As expected, the V4—O2′ distance opposite to V4—O5 is slightly elongated.

At room temperature the V4 site shows similar coordination with respect to V—O distances as the other octahedral V cations, although the average V—O distance for the $V4O_6$ octahedron is slightly smaller than for the remaining three octahedra. The coordination of V with respect to the next-nearest V neighbors is also similar for all four octahedra. Consequently, these interatomic distances do not give any indication why the V4 site should be favored by V^{4+} ions in the low-temperature phase. However, if one considers Yb—V interactions the V4 site is clearly different from the other three: while V1, V2 and V3 have four nearest Yb^{3+} neighbors at distances ranging between 3.0 and 4.2 Å, V4 has only three nearest Yb neighbors at, on average, shorter distances (Table 3). We believe that one of the underlying reasons for the phase transition in both polymorphs of YbV_4O_8 is exactly this difference in coordination, which might

[2] Madelung energy calculations carried out with the program *VESTA* (Momma & Izumi, 2008) do not indicate any order of V^{3+} and V^{4+} in the room-temperature phase, as the electrostatic energy per mole is basically identical for all four types of ordered models (−46.956, −47.002, −46.970 and −46.968 MJ mol^{-1} for V^{4+} at V1, V2, V3 and V4, respectively).

Table 3
Yb—V distances for α-YbV_4O_8 at room temperature (Kanke & Kato, 1997) and 8 K.

V1—Yb		V2—Yb		V3—Yb		V4—Yb	
290 K	8 K	290 K	8 K	290 K	8 K	290 K	8 K
3.0360 (3)	3.0168 (4)	3.4061 (3)	3.3960 (3)	4.0130 (3)	4.0302 (3)	3.3219 (3)	3.3336 (4)
3.6743 (3)	3.6344 (3)	3.3375 (3)	3.3423 (3)	3.9985 (3)	4.0264 (3)	3.3053 (3)	3.2869 (3)
4.0153 (3)	4.0914 (3)	4.1700 (3)	4.1719 (3)	3.7365 (3)	3.6690 (3)	3.1576 (3)	3.1572 (3)
4.0488 (3)	4.0719 (3)	4.1924 (3)	4.2136 (3)	3.0426 (3)	3.0446 (3)		

imply a lower Coulomb repulsion between Yb and V^{4+} for this site.

As discussed above, we assume the existence of a spin-singlet formation in the α' phase. This should be reflected in the corresponding V—V interactions. A detailed analysis shows that after the phase transition the V—V distances in the V1—V3 octahedral chain are slightly shortened, while distances in the V2—V4 octahedral chain are strongly elongated (Fig. 8, left). Consequently, we assume that as in the β' phase (Friese *et al.*, 2007), the spin-singlet formation takes place in the V1—V3 octahedral chain, which consists exclusively of trivalent V cations.

3.3. Comparison of the phase transition in the α and β polymorph

A comparison of the transitions $\alpha \rightarrow \alpha'$ and $\beta \rightarrow \beta'$ (Friese *et al.*, 2007) shows both transitions to be strikingly similar: in both cases the symmetry is not changed when passing the

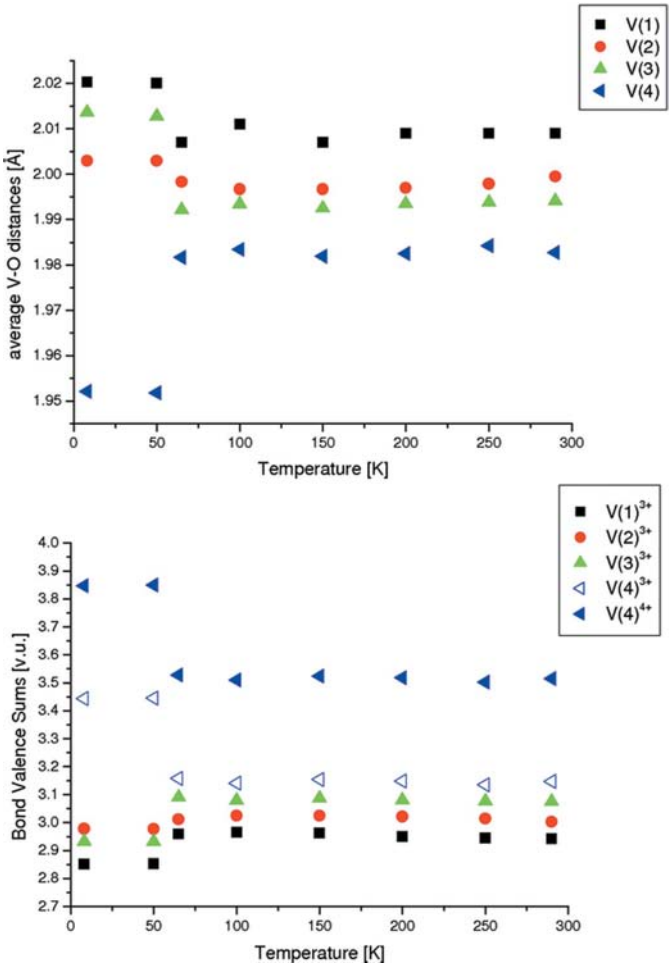

Figure 6
Average V—O distances in the octahedra and bond-valence sums according to Brese & O'Keeffe (1991) for α-YbV_4O_8 as a function of temperature. For V1, V2 and V3 the bond-valence sums have been calculated on the basis of an empirical parameter for V^{3+}; for V4 they have been calculated both on the basis of an empirical parameter for V^{3+} (open blue triangles) and V^{4+} (filled blue triangles). Standard deviations are smaller than the symbols indicated.

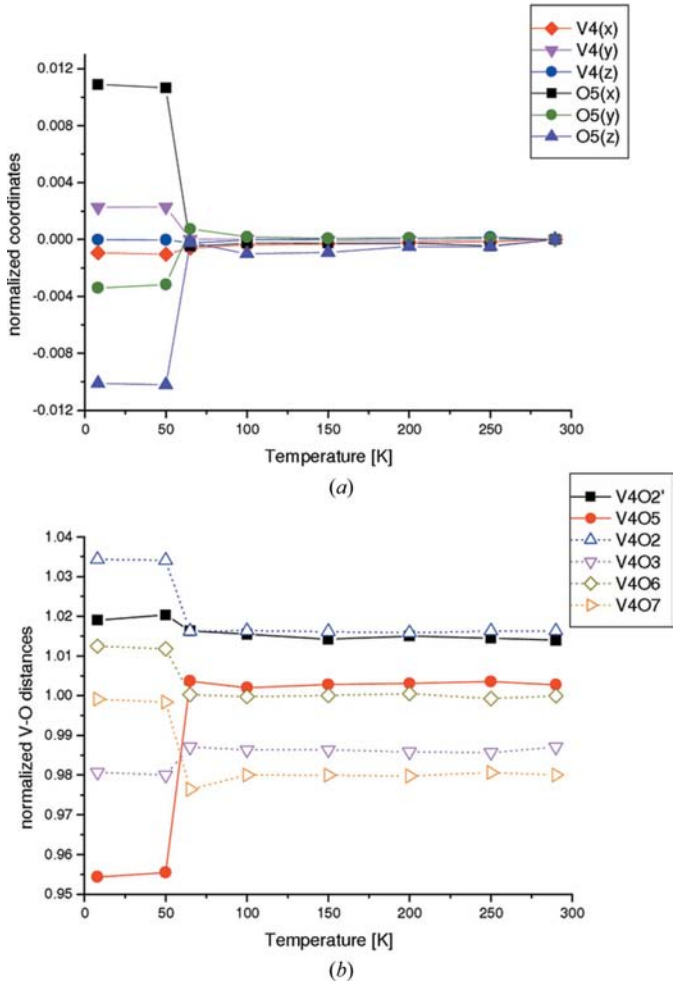

Figure 7
(*a*) Normalized coordinates of V4 and O5; (*b*) V4—O distances in the octahedra. The distances have been normalized with the average distance of the octahedra at each temperature point. The apical V—O distances characteristic of the vanadyl group are shown with solid lines and filled symbols. The other four equatorial V—O distances are shown with dotted lines and open symbols. Standard deviations are smaller than the symbols.

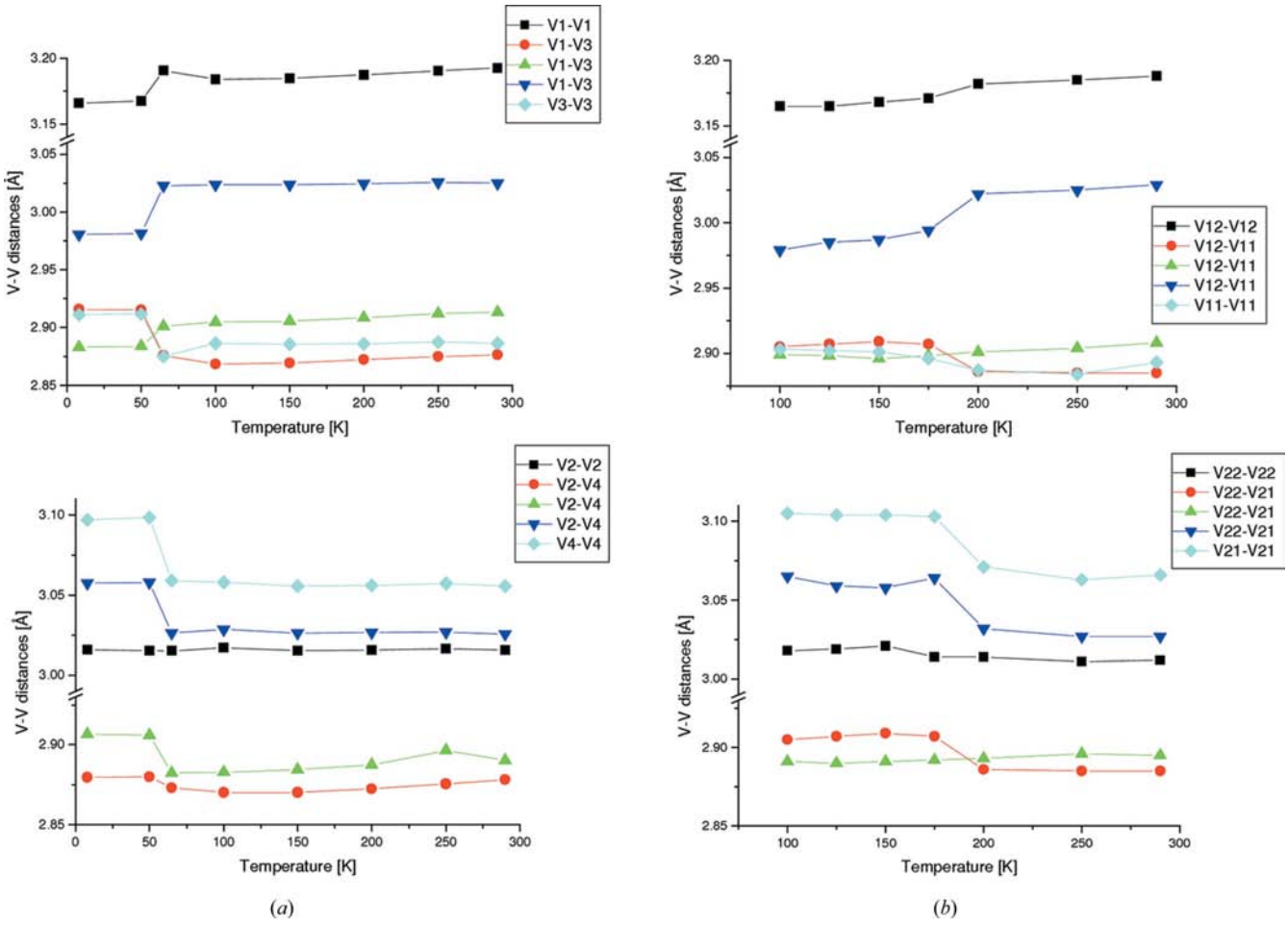

Figure 8
V—V distances in (*a*) α-YbV_4O_8 and (*b*) β-YbV_4O_8 as a function of temperature. Only the intrachain distances are shown. Standard deviations are in the range 0.0004–0.0005 Å for α-YbV_4O_8 and in the range 0.003–0.004 Å for β-YbV_4O_8.

transition and the transitions lead to a complete charge ordering of V^{3+} and V^{4+}. At both transitions there is an abrupt change of the unit-cell volume, the relative change being significantly larger at the $\alpha \rightarrow \alpha'$ transition when compared with the $\beta \rightarrow \beta'$ transition (0.25 and 0.18%).

Furthermore, a more detailed comparison of individual atomic distances results in surprising coincidences. Figs. 9 and 10 compare the octahedral V—O distances and the Yb—V distances, in the α and β polymorph.[3] Open symbols represent distances corresponding to the room-temperature phases, while filled symbols represent distances in the low-temperature phases (at 8 K for the α' and 100 K for the β' polymorph). It is evident that the Yb—V distances are extremely similar in the two polymorphs. A slightly larger variation is observed for the V—O distances. Naturally, the similarities in the distances both at high and low temperatures also imply that the respective phase transitions affect both structures in a more or less identical way.

The characteristic shortening of one of the V—O distances, leading to the formation of the vanadyl group mentioned above is also observed in β-YbV_4O_8, although the effect is not as dramatic as for α-YbV_4O_8: in the β phase the critical distance is shortened from 1.964 (9) Å at 200 K to 1.872 (8) Å at 175 K, while in the α phase the corresponding values are 1.989 (2) Å at 65 K and 1.8449 (18) Å at 50 K.

In both polymorphs the structural transitions are accompanied by magnetic anomalies. While the Curie constants obtained for the high-temperature regions are comparable, the Curie constant for the low-temperature region in the α' phase is slightly larger than in the β' phase. This implies that, assuming spin-gap formation for both low-temperature polymorphs, the ratio of (vanishing spin)/(surviving spin) in the α' phase should be smaller than the corresponding ratio for the β' phase. In this context it is interesting to compare the changes of individual V—V distances in detail as these should reflect the spin-gap formation.

As can be seen from Fig. 8, which shows the intrachain V—V distances as a function of temperature, the only distances which shrink at the transition to the low-temperature phases are in the V1—V3 chain in the α phase and in the V11—V12 chain in the β phase (Friese *et al.*, 2007). In both cases these

[3] Due to the similarities in the structures it is easy to pair the distances. Correspondences between the atoms in the α and α phase (Friese *et al.*, 2007), respectively, are: Yb ≡ Yb, V1 ≡ V12, V2 ≡ V22, V3 ≡ V11, V4 ≡ V21, O1 ≡ O12, O2 ≡ O21, O3 ≡ O31, O4 ≡ O41, O5 ≡ O11, O6 ≡ O22, O7 ≡ O32, O8 ≡ O42.

are the chains which incorporate only V^{3+} in the α' and β' phases, and the shortening of the distances suggests that the spin-gap formation takes place between V ions of these chains. Distances in the other chain, containing V^{4+} in the low-temperature phases (V2—V4 for α-YbV_4O_8 and V21—V22 for β-YbV_4O_8), are either not affected by the transition or are significantly elongated with decreasing temperature. The most pronounced decrease is observed for one of the three V1—V3 distances (V11—V12 in the β polymorph), the decrease being comparable for the two polymorphs. In addition, the V1—V1/V12—V12 distances are very slightly shortened with decreasing temperature. The other three relevant distances have slightly different behaviors in the α and β phase. The V3—V3/V11—V11 and one of the remaining V1—V3/V11—V12 distances increase at the transition, the increase being significantly larger for the α phase. The third V1—V3 distance decreases in the α phase, while the corresponding V11—V12 distance stays constant at the $\beta \rightarrow \beta'$ transition. These observations suggest that the spin-gap formation follows the same mechanism in both polymorphs.

Given the very similar structures and behaviors of the two polymorphs, the question arises why the transition temperature of the α polymorph is approximately 120 K lower than for the β polymorph.

Assuming that electrostatic repulsion between V^{4+} and Yb^{3+} is one of the driving forces of the phase transition, any initial differences in the degree of ordering of V^{3+} and V^{4+} could play a key role in explaining the difference in transition temperature. It is thus interesting to notice that the bond-valence sums of the octahedral sites in the α and β polymorph at ambient temperature are slightly different. In particular, the bond-valence sum for the V4 site in the α phase is slightly lower than for the corresponding vanadium site in the β phase (3.217 v.u. compared with 3.246 v.u. using an empirical parameter for V^{3+}; Friese *et al.*, 2007). As these octahedra incorporate the V^{4+} after the $\alpha \rightarrow \alpha'$ and $\beta \rightarrow \beta'$ transitions, respectively, this fact might be related to the lower transition temperature in α-YbV_4O_8. In any case, the structural differences which stabilize the α polymorph in comparison to the β polymorph must be very subtle and probably involve not only first- and second-nearest, but even third-nearest neighbor interactions.

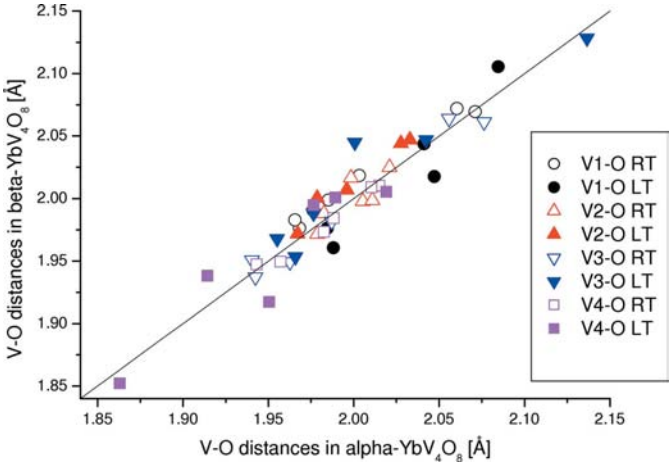

Figure 9
V—O distances in the octahedra. Distances for the α and β phase at 290 K are shown as open symbols; distances for α' (8 K) and β' (100 K) are indicated by filled symbols.

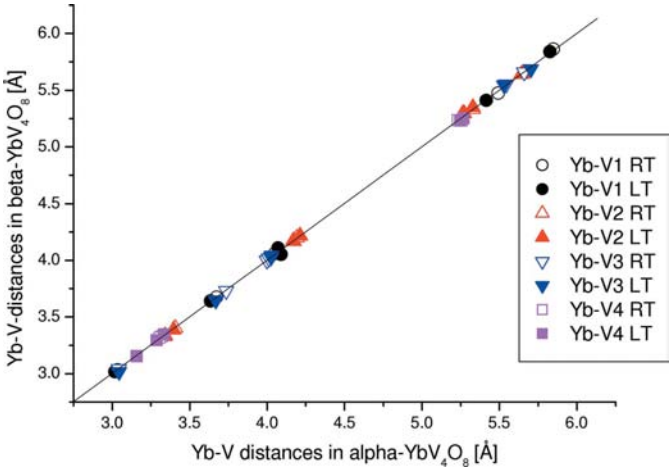

Figure 10
Yb—V distances up to 6 Å. Distances for the α and β phase at 290 K are shown as open symbols; distances for α' (8 K) and β' (100 K) are indicated by filled symbols.

4. Conclusions

We have shown that the isosymmetrical phase transition in α-YbV_4O_8 is comparable to the transition observed in the β polymorph. Although this might be a result to be expected given the similarities of the structures, the extremely high degree of coincidence of geometrical parameters is surprising. Both transitions lead to complete charge ordering of the three V^{3+} and one V^{4+}. The lower transition temperature of the α polymorph when compared with the β polymorph might be related to the fact that less positive charge is concentrated at the key octahedral site at room temperature.

The first-order transition in α-YbV_4O_8 involves huge shifts of the atoms, of similar magnitude to those observed in the isostructural transition of multiferroic hexagonal manganites, which show giant magnetoelastic coupling (Lee *et al.*, 2008). In the manganites the isostructural transitions are related to the onset of antiferromagnetic ordering. In α-YbV_4O_8, however, the structural transition is associated with a paramagnetic–paramagnetic anomaly, which most probably involves additional spin-singlet formation.

Financial support by the Ministerio de Educación y Ciencia, the Gobierno Vasco and the Universidad del País Vasco is acknowledged. This work was supported by the European Community Research Infrastructure Action under the FP6-Programs: Structuring the European Research Area, through the Integrated Infrastructure Initiative Integrating Activity on Synchrotron and Free Electron Laser Science, (IA-SFS).

References

Alonso, J. A., García-Muñoz, J. L., Fernández-Díaz, M. T., Aranda, M. A. G., Martínez-Lope, M. J. & Casais, M. T. (1999). *Phys. Rev. Lett.* **82**, 3871–3874.

Becker, P. J. & Coppens, P. (1974). *Acta Cryst.* A**30**, 129–147.

Berry, F. J., Skinner, S. & Thomas, M. F. (1998). *J. Phys. Condens. Matter*, **10**, 215–220.

Brese, N. E. & O'Keeffe, M. (1991). *Acta Cryst.* B**47**, 192–197.

Daoud-Aladine, A., Rodríguez-Carvajal, J., Pinsard-Gaudart, L., Fernández-Díaz, M. T. & Revcolevschi, T. (2002). *Phys. Rev. Lett.* **89**, 097205.

Friese, K., Jarchow, O., Kato, K. & Kanke, Y. (1997). *Z. Kristallogr.* **212**, 859–863.

Friese, K., Kanke, Y., Fitch, A. N. & Grzechnik, A. (2007). *Chem. Mater.* **19**, 4882–4889.

Goff, R. J. & Attfield, J. P. (2004). *Phys. Rev. B*, **70**, 140404.

Hinrichsen, B., Dinnebier, R. E. & Jansen, M. (2006). *Z. Kristallogr. Suppl.* **23**, 231–236.

Kanke, Y. & Kato, K. (1997). *Chem. Mater.* **9**, 141–147.

Kato, K., Kanke, Y. & Friese, K. (1997). *Z. Kristallogr.* **212**, 110–114.

LeBail, A., Duroy, H. & Fourquet, J. L. (1988). *Mater. Res. Bull.* **23**, 447–452.

Lee, S., Pirogov, A., Kang, M., Jang, K.-H., Yonemura, M., Kamiyama, T., Cheong, S.-W., Gozzo, F., Shin, N., Kimura, H., Noda, Y. & Park, J. (2008). *Nature*, **451**, 805–808.

Momma, K. & Izumi, F. (2008). *J. Appl. Cryst.* **41**, 653–658.

Nagaev, E. L. (2002). *Colossal Magnetoresistance and Phase Separation in Magnetic Semi-conductors.* London: Imperial College Press.

Onoda, M., Dhaussy, A.-C. & Kanke, Y. (2003). *Acta Cryst.* B**59**, 429–438.

Petříček, V., Dušek, M. & Palatinus, L. (2006). *JANA*2006. Institute of Physics, Praha, Czech Republic.

Radaelli, P. G., Cox, D. E., Mareizo, M. & Cheong, S. W. (1997). *Phys. Rev. B*, **55**, 3015–3023.

Rao, C. N. R., Arulraj, A., Santosh, P. N. & Cheetham, A. K. (1998). *Chem. Mater.* **10**, 2714–2722.

Samiullah, M. (1995). *Phys. Rev. B*, **51**, 10352–10356.

Vogt, T., Woodward, P. M., Karen, P., Hunter, B. A., Henning, P. & Moodenbaugh, A. R. (2000). *Phys. Rev. Lett.* **84**, 2969–2972.

Woodward, P. M., Cox, D. E., Moshopoulou, E., Sleight, A. W. & Morimoto, S. (2000). *Phys. Rev. B*, **62**, 844–855.